THE JOURNAL OF PHYSICAL CHEMISTRY B LETTERS

**2006,** *110,* 21394−21398
Published on Web 10/10/2006

# Formation of a Regular Fullerene Nanochain Lattice

**Wende Xiao,[†] Pascal Ruffieux,[†] Kamel Aït-Mansour,[†] Oliver Gröning,[†] Krisztian Palotas,[‡] Werner A. Hofer,[‡] Pierangelo Gröning,[†] and Roman Fasel*,[†]**

*Empa, Swiss Federal Laboratories for Materials Testing and Research, nanotech@surfaces Laboratory, Feuerwerkerstrasse 39, CH-3602 Thun, Switzerland, and Surface Science Research Centre, The University of Liverpool, Liverpool L69 3bX, United Kingdom*

*Received: August 17, 2006; In Final Form: September 22, 2006*

A vicinal Au(11 12 12) surface, naturally patterned into a rectangular superlattice, has been used as a template to prepare $C_{60}$ nanostructures with long-range order and uniform size. At a coverage of 0.1 monolayer and at room temperature, a two-dimensional long-range ordered superlattice of molecular nanochains is achieved, which perfectly replicates the periodicity of the template surface. The fullerene nanochains are found to be located exclusively on the face-centered cubic stacking domains at the lower step edges. Our experiments demonstrate that highly periodic molecular nanochains can be fabricated through a site-selective anchoring method.

## 1. Introduction

Organic nanoscale structures on surfaces with long-range order and uniform size have attracted considerable attention in recent years,[1−3] motivated by potential applications in micro- and optoelectronic devices, which exploit the flexibility of molecular structure and properties.[2] To overcome the essential disadvantages of limited minimum feature size and low throughput of ultimate-resolution lithographic methods, the application of self-assembly techniques is widely expected to efficiently generate large-scale nanostructures out of prefabricated molecular building blocks with intrinsic physical and chemical properties. The controllable fabrication of highly ordered homogeneous nanostructures on surfaces, however, remains a difficult challenge.

To achieve well-ordered and rather uniform metallic nanostructure arrays on surfaces, the use of patterned substrates has been reported.[4] It has been demonstrated that substrates exhibiting strain relief and dislocation networks can serve as excellent templates.[5] The underlying mechanism is due to the lateral inhomogeneity of the template surface.[4] The initial nucleation of deposited atoms occurs preferentially in some regions, and these special sites can be viewed as "anchor sites". Therefore, surfaces with well-ordered uniform arrays of anchor sites are promising templates for the fabrication of extremely regular nanostructures via site-selective nucleation and ensuing self-assembly.

It is well-known that steps, kinks, impurities, and other defect sites on surfaces can serve as anchor sites for adsorbed molecules. Vicinal surfaces are thus natural templates for growing regularly spaced uniform nanostructures, as the straight steps separated by uniform terraces run parallel to each other on the entire surface area. Recently, Rousset and co-workers systematically investigated a variety of vicinal Au(111) surfaces and found that the stable Au(788) and Au(11 12 12) surfaces are rectangular superlattices consisting of monatomic steps and discommensuration lines,[6,7] which derive from the $22\times\sqrt{3}$ "herringbone" reconstruction of the Au(111) terraces.[8,9] Both substrates have successfully been applied as templates for the growth of long-range ordered Co nanodot arrays.[10,11]

Since shortly after its discovery in 1985,[12] the adsorption of $C_{60}$ and related compounds on metal surfaces,[13] particularly on Au(111), has been extensively investigated. By now, it is well-known that $C_{60}$ is mobile on flat Au(111) terraces at room temperature (RT) and diffuses to the step edges where it is immobilized on face-centered cubic (fcc) stacking areas.[14,15] Hence, the selective anchoring at step edges makes the $C_{60}$ molecule an excellent candidate for site-selective anchoring on a Au(11 12 12) template surface.

In this work, we used the Au(11 12 12) surface as a template to prepare $C_{60}$ nanostructures with long-range order and uniform size. We observed the formation of an extended superlattice of regular short molecular chains of $C_{60}$, which follows the lattice of the template. The exact location of the molecular nanochains on the substrate is identified by means of in situ ultrahigh vacuum (UHV) variable-temperature (VT) scanning tunneling microscopy (STM) and low-energy electron diffraction (LEED).

## 2. Experimental Section

Experiments were carried out in a UHV VT-STM system (Omicron) equipped with a LEED and standard surface preparation facilities. The nominal single-crystal Au(11 12 12) (Surface Preparation Laboratory, Netherlands) was prepared using repeated cycles of sputtering with argon ions (typically at an argon pressure of $2 \times 10^{-5}$ mbar, an acceleration voltage of 750 V, and an incidence angle of $<10°$ along the step direction) and annealing at ∼800 K, similar to the procedure described by

* To whom correspondence may be addressed. E-mail: roman.fasel@empa.ch.
[†] Swiss Federal Laboratories for Materials Testing and Research.
[‡] The University of Liverpool.

10.1021/jp065333i CCC: $33.50 

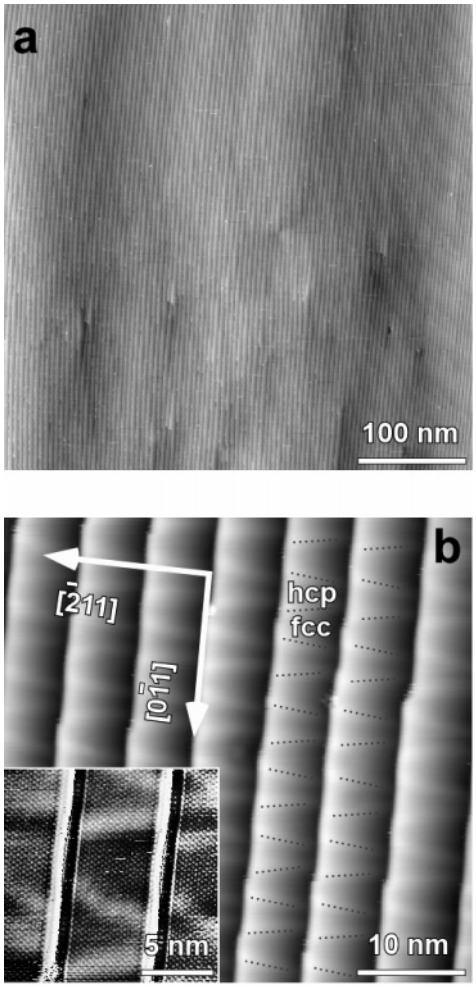


**Figure 1.** RT STM images of the Au(11 12 12) template surface: (a) overview showing regular straight steps on a 500 × 500 nm length scale (−0.05 V, 0.6 nA); (b) higher-magnification image (−2 V, 0.1 nA) highlighting the 2D superlattice of steps and discommensuration lines separating fcc and hcp stacking areas. The inset (−1.6 V, 0.5 nA) shows an atomic resolution image with a maximum grayscale contrast applied to each terrace individually.

Repain et al.[10] Before the deposition of $C_{60}$, cleanliness and surface order were monitored by STM and LEED. $C_{60}$ molecules were sublimated from a Knudsen-cell-type evaporator at a temperature of 670 K, while the Au(11 12 12) substrate was held at RT. STM images were acquired in constant-current mode either at RT or at a sample temperature of 40 K.

### 3. Results and Discussion

After surface preparation, the clean Au(11 12 12) exhibits excellent long-range order of both the step edge sequence and the reconstruction lines on a mesoscopic length scale. Large-scale STM images such as the one displayed in Figure 1a reveal a highly regular array of monatomic steps. A Fourier analysis of a series of STM images yields a superlattice periodicity of $a = 7.2 \pm 0.2$ nm along the steps and $b = 5.8 \pm 0.2$ nm across the terraces. These values are precisely the ones of the ideal Au(11 12 12) template surface,[7] which exhibits 5.8 nm wide terraces and 7.2 nm spaced discommensuration lines. The high-magnification STM image shown in Figure 1b clearly demonstrates the straight steps and the discommensuration lines on the terraces, which derive from the $22\times\sqrt{3}$ reconstruction of the Au(111) surface.[8,9] The bright lines are ridges of surface atoms occupying bridge sites, which separate fcc and hexagonal close-packed (hcp) stacking regions.[9] The array of steps and discommensuration lines forms a two-dimensional (2D) pattern. We note that there are very few kinks along the steps, which reflects that the overall step direction deviates only slightly from the close-packed [0$\bar{1}$1] direction. The inset shows an atomic resolution image where the corrugation due to the discommensuration lines is also clearly visible. It is seen that each terrace consists of 24 parallel atomic rows. Interestingly, the steps are not perfectly straight on this length scale, but, in fcc regions of the upper terrace, the atoms of the row near the step edge appear to stretch out up to 1.8 ± 0.4 Å more than the ones in hcp regions. We attribute this to a partial release of the stress induced by the $22\times\sqrt{3}$ reconstruction, which is stronger in fcc than in hcp regions. As noted previously,[7] the discommensuration lines do not run perpendicular to the close-packed direction on the narrow terraces. It can be seen from Figure 1b that these lines form a truncated "V" shape, resulting in an increase of the width of the fcc domains approaching the lower part of the step edge. On the other hand, the row of atoms near the lower step edge appears ∼0.24 ± 0.04 Å higher than its neighbors in the middle of the terrace, which we attribute to a slight electron excess in this region.[16]

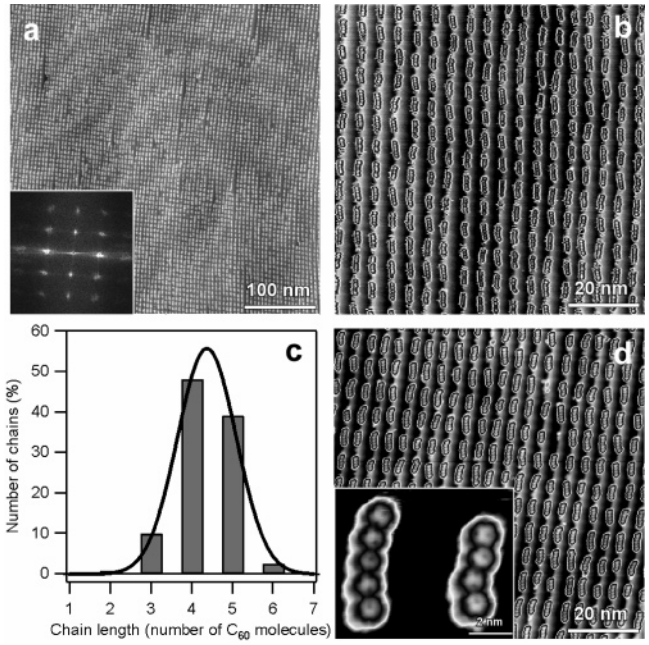


**Figure 2.** Formation of a highly regular 2D superlattice of $C_{60}$ nanochains on the Au(11 12 12) template surface after RT deposition of ∼0.1 ML $C_{60}$: (a) overview (500 × 500 nm, −1 V, 0.03 nA) and corresponding Fourier power spectrum; (b) RT STM image (−1.5 V, 0.02 nA) resolving the individual $C_{60}$ molecules forming the nanochains; (c) length distribution of the $C_{60}$ chains; (d) STM image taken at a sample temperature of ∼40 K (−2 V, 0.03 nA), where the $C_{60}$ molecules are frozen at the step edges. The inset (−2.5 V, 0.5 nA) shows an intramolecular resolution image of two short chains. To enhance the visibility of individual $C_{60}$ molecules, the images shown in panels b and d are given in a double grayscale representation.

Figure 2a shows the morphology after the deposition of roughly 0.1 monolayer (ML) $C_{60}$ on the Au(11 12 12) template surface at RT. Here, 1 ML $C_{60}$ refers to a complete close-packed molecular layer on the Au(11 12 12) surface, as estimated with STM. It is seen that the surface consists of an extremely regular 2D superlattice of short molecular chains. The high degree of long-range order is confirmed by very sharp LEED patterns (not shown) and the STM Fourier power spectrum (inset in Figure 2a). A Fourier analysis reveals that the nanochain superlattice parameters correspond to those of the template surface, namely,

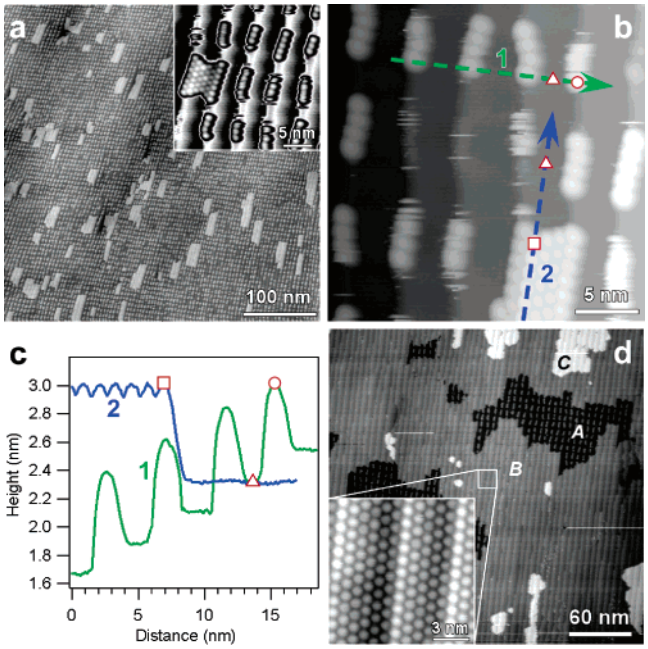


**Figure 3.** Formation of 2D $C_{60}$ islands at coverages above 0.1 ML. (a) RT STM image showing the formation of small islands after $C_{60}$ deposition of ~0.15 ML (500 × 500 nm, −0.5 V, 0.02 nA). The inset (−1 V, 0.02 nA) shows the smallest island observed, which extends from the lower step edge of one terrace to the lower step edge of the adjacent terrace. (b,c) Line profiles across short chains at the step edges (1), and along a $C_{60}$ island on the terrace (2). (d) RT STM image after deposition of ~1 ML $C_{60}$ (−2.2 V, 0.03 nA), showing the coexistence of areas consisting of fullerene nanochains (A), extended regions covered by a close-packed $C_{60}$ monolayer (B, inset), and second layer islands (C).

$a = 7.2 \pm 0.2$ nm and $b = 5.8 \pm 0.2$ nm. Zoom-in scans (e.g., Figure 2b) show that the $C_{60}$ molecules are adsorbed at the step edges of the substrate, which is consistent with previous reports of high $C_{60}$ mobility on flat Au(111) terraces.[14] A detailed analysis reveals that 85% of the molecular chains consist of four or five $C_{60}$ molecules, as shown in Figure 2c. The shortest and longest chains include two and six $C_{60}$ molecules, respectively. Single $C_{60}$ molecules are observed neither on terraces nor at step edges. This is in line with previous observations that $C_{60}$ molecules tend to bind with each other and that dimers and large aggregates are immobile at step edges at RT.[14] However, the binding between $C_{60}$ molecules and the Au substrate is not strong enough to prevent occasional instabilities when scanning at RT. Although a reasonably high sample bias of approximately −2.7 V and a low tunneling current of ~0.02 nA are applied, the disturbance from the tip during scanning results in frequent displacements of $C_{60}$ molecules from the molecular nanochains, as evidenced by the short horizontal streaks in Figure 2b. At a temperature of 40 K, however, the $C_{60}$ molecules are frozen at the step edges, resulting in stable imaging conditions (Figure 2d). Low-temperature STM images with $C_{60}$ intramolecular resolution, as shown in the inset of Figure 2d, reveal the orientations of the molecules, as previously reported.[17] We note that, already at $C_{60}$ coverages below 0.1 ML, most $C_{60}$ nanochains consist of three to five molecules, although there are still many empty fcc domain step edge segments available.

To clarify the exact location of the $C_{60}$ nanochains with respect to the step edges, we have prepared samples with a slightly higher coverage of ~0.15 ML. As shown in Figure 3a, small patches of hexagonally close-packed $C_{60}$ islands of monolayer height can be observed at this coverage. Line profiles (Figure 3b,c) disclose that the apparent height of $C_{60}$ molecules relative to the lower terrace of the step edges is about 7 Å. The same height is measured for molecules of the small island on the terrace, confirming that the $C_{60}$ nanochains are located on the lower terrace of the step edges. The inset of Figure 3a shows short molecular chains and one of the smallest islands, which extends from the lower step edge of one terrace to the lower step edge of the adjacent terrace. Line profiles across this island (not shown) reveal that the $C_{60}$ molecules adsorbed at the step edges appear ~0.8 Å higher than their neighbors within the island, which has been attributed to a modification of molecular bonding at step edges due to the formation of electron-deficient and electron-rich regions above and below the step edge, respectively.[16,18]

To further investigate the growth mode, we prepared a series of samples with coverages ranging from 0.1 ML to above full monolayer coverage. With increasing coverage, the small islands shown in Figure 3a laterally grow in size and coalesce to an extended hexagonally close-packed layer. Apart from the one-dimensional (1D) nanochains consisting of four to five molecules, there is no other preferred, stable island size. The nanochain lattice, however, is surprisingly stable and persists up to high coverages. At nominal 1 ML coverage (Figure 3d), surface areas consisting of the regular nanochain lattice (A) coexist with extended monolayer regions (B) and first patches of the second $C_{60}$ layer (C). A 2D wetting of the template surface is thus energetically preferred over a closing of the nanochain segments into extended 1D molecular chains.

Figure 4a shows a close-up of two nanochains imaged at 40 K. On the adsorbate-free regions of the terraces, the discommensuration lines can be discerned as white corrugations. It is seen that $C_{60}$ nanochains are exclusively located on the fcc areas between two discommensuration lines. Therefore, the small $C_{60}$ island near the left border of the inset of Figure 3a exactly occupies one fcc domain with the leftmost molecular row on the adjacent lower terrace. Interestingly, the $C_{60}$ chains shown in Figure 4a appear to be embedded within the steps, rather than being located on the lower terrace at the step edges. As outlined above, however, their apparent height is only consistent with the latter location, on the lower terraces at the lower step edges. To clarify these seemingly contradictory observations, we performed STM simulations for a clean Au(111) surface with a {111} microfaceted step, representative of the steps of the Au(11 12 12) surface. After a self-consistent calculation of the step electronic structure within density functional theory, VASP,[19] STM images were simulated within the first-order scattering approach of electron tunneling implemented in the BSKAN code.[20] A line profile across the step edge, simulated for the experimental tunneling parameters of $I_t = 0.02$ nA and $U_g = -1.0$ V is given in Figure 4c (black curve). Because of the extended Au charge density, the step edge of the simulated STM line profile appears to be shifted away from the step atomic position by 3.2 Å. This shift is observed to be highly bias dependent and depends also on the tip. Considering a finite tip apex shifts the apparent edge position further away from the location of the geometrical step edge. For a spherical tip apex of 1 nm radius, we find the apparent step edge position 5.7 Å away from the center of the step atoms (Figure 4c). The effect of a finite tip size on the imaging of asymmetric features such as step edges is thus a shift of the apparent location away from the "true" geometrical location. For a symmetric topographic feature, however, such as an adsorbed $C_{60}$ molecule, a finite tip apex broadens the image but conserves the apparent location. This perfectly explains why the $C_{60}$ molecule (line profile 1) is

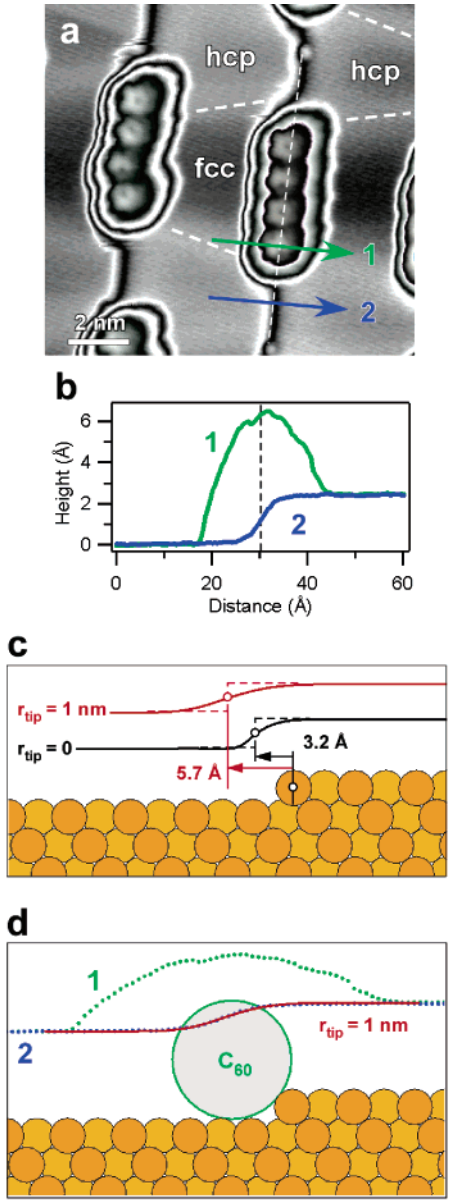


**Figure 4.** Location of $C_{60}$ nanochains on fcc domains at the lower step edges. (a) STM image taken at ~40 K (11.5 × 12 nm, −2.5 V, 0.5 nA). Arrows indicate the origin of line profiles 1 and 2 shown in panel b. (c) Simulated STM line profiles across a step edge, for an infinitely sharp tip (black) and a spherical tip apex of 1 nm radius (red). (d) Comparison of an experimental step edge STM line profile (2) and a simulation (red). The apparent step edge position coincides with the position of the $C_{60}$ molecule (1), which explains the STM picture given in panel a, where the $C_{60}$ nanochains seem to be embedded within the steps.

imaged at the same location as the step edge (profile 2), although its geometrical location (center of $C_{60}$ sphere) is a few angstroms away from the step edge, as shown in Figure 4d. We note that this asymmetry should always be carefully considered when interpreting STM images from molecules adsorbed at or near step edges.

In line with our observations of a regular $C_{60}$ nanochain lattice on the Au(11 12 12) template surface, the formation of long-range ordered Co nanodot arrays on the stepped Au(788) surface was reported.[10,11] VT-STM experiments and theoretical calculations indicated that the ordered growth of Co nanodots on Au(788) originates from the presence of preferred adsorption/nucleation sites on the template surface.[10] In principle, an analogous explanation can be put forward to rationalize the formation of a regular $C_{60}$ nanochain lattice on Au(11 12 12). Simply considering that the lower part of the step edge provides a higher coordination than the upper part suggests that preferential adsorption of $C_{60}$ occurs there to minimize the total energy.[18] Furthermore, the region of a terrace near the lower step edge is electron-rich according to the Smoluchowski effect,[16] and $C_{60}$ is well-known as an electron acceptor, leading to the possibility of charge transfer and strong binding at these sites. The observation that close-packed $C_{60}$ islands only grow after complete decoration of the step edges in fcc stacking areas (Figure 3) allows an estimate of the step edge contribution to the $C_{60}$ adsorption energy. While the molecules at the edges of a close-packed $C_{60}$ island linking two nanochains (Figure 3a, inset) exhibit a cohesive energy of about 0.87 eV (2/3 of the $C_{60}$ monolayer cohesive energy of 1.31 eV),[21] molecules within linear chains at step edges are only 1 or 2-fold coordinated, corresponding to cohesive energies of about 0.22 eV or 0.44 eV, respectively. Adsorption at step edges is thus energetically favored by about 0.43−0.65 eV compared to adsorption on flat terraces.

On the other hand, the electronic potential energy of the Au(23 23 21) fcc regions was reported to be 92 meV higher than that of the hcp stacking areas,[22] indicating a higher reactivity. Therefore, a stronger binding of $C_{60}$ to fcc domain areas can be expected, resulting in a preferential accommodation of $C_{60}$ molecules on fcc domains. A similar selective decoration of fcc domains of Au(111) steps by 1-nitronaphthalene molecules was observed experimentally and was theoretically explored by first-principles calculations.[23] The width of the fcc domains near the lower step edges is measured to be 4.3 ± 0.1 nm (Figure 4a), large enough to host $C_{60}$ chains consisting of four to five $C_{60}$ molecules with an intermolecular distance of about 1 nm. In this way, the periodicity of the template surface is transferred into an array of short chains of $C_{60}$ molecules, and a long-ranged ordered nanochain superlattice is achieved with a very uniform size distribution. At higher coverages, the $C_{60}$ layer grows out from the chains across the terraces, which is thus energetically preferred over a closing of the nanochain segments into extended 1D molecular chains.

The observation of nanochain formation followed by 2D growth initiated by terrace filling between nanochain segments on adjacent step edges is contradictory to a report on the formation of a fullerene nanomesh on Au(788), which was published during the completion of this manuscript.[24] While Berndt and co-workers also observed an initial nucleation of $C_{60}$ on fcc stacking areas at step edges, higher $C_{60}$ coverage was reported to result in the formation of noncoalescing rectangular islands: four $C_{60}$ chains wide and four to five molecules long. As is clearly seen from Figure 3, there is definitely no formation of isolated 2D islands on Au(11 12 12) giving rise to a "nanomesh", but rather a continuous lateral growth of extended fullerene islands covering larger and larger surface areas. This difference might be attributed to the different terrace widths of the two vicinal surfaces: whereas Au(11 12 12) exhibits 5.8 nm wide terraces, the ones of the Au(778) measure only 3.8 nm. However, we also did not observe noncoalescing islands on surface areas with similarly narrow terraces, for example, in areas with step bunches or deviations from the nominal (11 12 12) orientation. We also note that the interpretation of Berndt and co-workers regarding the location of $C_{60}$ chains with respect to the step edge must have been performed without taking into account the asymmetric imaging induced by the finite tip size, as discussed in detail above.

## 4. Conclusions

In summary, we have successfully prepared $C_{60}$ nanostructures with long-range order and uniform size on a Au(11 12 12)

template surface. The periodicity of this template is replicated to a superlattice of regular $C_{60}$ nanochains. The almost monodisperse $C_{60}$ chains are found to be located exclusively on the fcc stacking domains at the lower part of the step edges. These observations constitute a successful proof-of-principle for the concept of site-selective molecular anchoring on nanostructured template surfaces, and provide the perspective of fabricating complex supramolecular nanostructures being of potential technological relevance by site-selective anchoring and self-assembly methods using properly designed functional molecular building blocks.

**Acknowledgment.** Financial support by the European Commission (RADSAS, NMP3-CT-2004-001561) is gratefully acknowledged.

## References and Notes

(1) De Feyter, S.; De Schryver, F. C. *Chem. Soc. Rev.* **2003**, *32*, 139.

(2) Rosei, F.; Schunack, M.; Naitoh, Y.; Jiang, P.; Gourdon, A.; Laegsgaard, E.; Stensgaard, I.; Joachim, C.; Besenbacher, F. *Prog. Surf. Sci.* **2003**, *71*, 95.

(3) Barlow, S. M.; Raval, R. *Surf. Sci. Rep.* **2003**, *50*, 201.

(4) Brune, H. *Surf. Sci. Rep.* **1998**, *31*, 121.

(5) Brune, H.; Giovannini, M.; Bromann, K.; Kern, K. *Nature (London)* **1998**, *394*, 451.

(6) Mugarza, A.; Mascaraque, A.; Pérez-Dieste, V.; Repain, V.; Rousset, S.; García de Abajo, F. J.; Ortega, J. E. *Phys. Rev. Lett.* **2001**, *87*, 107601.

(7) Rousset, S.; Repain, V.; Baudot, G.; Garreau, G.; Lecoeur, J. *J. Phys.: Condens. Matter* **2003**, *15*, S3363.

(8) (a) Harten, U.; Lahee, A. M.; Toennies, J. P.; Wöll, Ch. *Phys. Rev. Lett.* **1985**, *54*, 2619. (b) Wöll, Ch.; Chiang, S.; Wilson, R. J.; Lippel, P. H. *Phys. Rev. B* **1989**, *39*, 7988.

(9) Barth, J. V.; Brune, H.; Ertl, G.; Behm, R. J. *Phys. Rev. B* **1990**, *42*, 9307.

(10) (a) Repain, V.; Berroir, J. M.; Rousset, S.; Lecoeur, J. *Surf. Sci.* **2000**, *447*, L152. (b) Repain, V.; Baudot, G.; Ellmer, H.; Rousset, S. *Europhys. Lett.* **2002**, *58*, 730. (c) Repain, V.; Baudot, G.; Ellmer, H.; Rousset, S. *Mater. Sci. Eng., B* **2002**, *96*, 178. (d) Rohart, S.; Baudot, G.; Repain, V.; Girard, Y.; Rousset, S.; Bulou, H.; Goyhenex, C.; Proville, L. *Surf. Sci.* **2004**, *559*, 47. (e) Witkowski, N.; Borensztein, Y.; Baudot, G.; Repain, V.; Girard, Y.; Rousset, S. *Phys. Rev. B* **2004**, *70*, 85408.

(11) Shiraki, S.; Fujisawa, H.; Nantoh, M.; Kawai, M. *Appl. Surf. Sci.* **2004**, *237*, 284.

(12) Kroto, H. R.; Heath, J. R.; O'Brien, S. C.; Curl, R. F.; Smalley, R. E. *Nature (London)* **1985**, *318*, 162.

(13) Pedio, M.; Hevesi, K.; Zema, N.; Capozi, M.; Perfetti, P.; Gouttebaron, R.; Pireaux, J.-J.; Caudano, R.; Rudolf, P. *Surf. Sci.* **1999**, *437*, 249.

(14) Altman, E. I.; Colton, R. J. *Surf. Sci.* **1992**, *279*, 49.

(15) Fujita, D.; Yakabe, T.; Nejoh, H.; Sato, T.; Iwatsuki, M. *Surf. Sci.* **1996**, *366*, 93.

(16) Smoluchowski, R. *Phys. Rev.* **1941**, *60*, 661.

(17) (a) Hou, J. G.; Yang, J.; Wang, H.; Li, Q.; Zeng, C.; Lin, H.; Wang, B.; Chen, D. M.; Zhu, Q. *Phys. Rev. Lett.* **1999**, *83*, 3001. (b) Pascual, J. I.; Gómez-Herrero, J.; Rogero, C.; Baró, A. M.; Sánchez-Portal, D.; Artacho, E.; Ordejón, P.; Soler, J. M. *Chem. Phys. Lett.* **2000**, *321*, 78.

(18) Rogero, C.; Pascual, J. I.; Gómez-Herrero, J.; Baró, A. M. *J. Chem. Phys.* **2002**, *116*, 832.

(19) Kresse, G.; Furthmüller, J. *Phys. Rev. B* **1996**, *54*, 11169.

(20) Palotás, K.; Hofer, W. A. *J. Phys.: Condens. Matter* **2005**, *17*, 2705.

(21) Nakamura, J.; Nakayama, T.; Watanabe, S.; Aono, M. *Phys. Rev. Lett.* **2001**, *87*, 48301.

(22) Didiot, C.; Fagot-Revurat, Y.; Pons, S.; Kierren, B.; Chatelain, C.; Malterre, D.; *Phys. Rev. B* **2006**, *74*, 81404.

(23) Vladimirova, M.; Stengel, M.; De Vita, A.; Baldereschi, A.; Böhringer, M.; Morgenstern, K.; Berndt, R.; Schneider, W.-D. *Europhys. Lett.* **2001**, *56*, 254.

(24) Néel, N.; Kröger, J.; Berndt, R. *Adv. Mater.* **2006**, *18*, 174.